

Hyperbolic chaos in a system of two Froude pendulums with alternating periodic braking

Sergey P. Kuznetsov^{1,2} and Vyacheslav P. Kruglov²

¹ Udmurt State University, Universitetskaya 1, Izhevsk, 426034 Russia.

² Kotel'nikov Institute of Radio Engineering and Electronics, Russian Academy of Sciences, Saratov Branch, Zelenaya 38, Saratov, 410019 Russia.

We propose a new example of a system with a hyperbolic chaotic attractor. The system is composed of two coupled Froude pendulums placed on a common shaft rotating at constant angular velocity with braking by application of frictional force to one and other pendulum turn by turn periodically. A mathematical model is formulated and its numerical study is carried out. It is shown that attractor of the Poincaré stroboscopic map in a certain range of parameters is a Smale – Williams solenoid. The hyperbolicity of the attractor is confirmed by numerical calculations analyzing the angles of intersection of stable and unstable invariant subspaces of small perturbation vectors and verifying absence of tangencies between these subspaces.

Hyperbolic theory is a section of the theory of dynamical systems that provides a rigorous mathematical justification for chaotic behavior of deterministic systems, both with discrete time (maps) and with continuous time (flows) [1-4]. The creation of this theory was, as said by D.V. Anosov, the content of the "hyperbolic revolution" of the 60s of the XX century [5].

If we talk about dissipative chaotic systems, the hyperbolic theory introduces a special type of attracting invariant sets, the uniformly hyperbolic attractors composed exclusively of saddle phase trajectories. For all points on such a trajectory in the space of small perturbations (tangent space), we can define a subspace of vectors exponentially decreasing in norm in direct time, and a subspace of vectors exponentially decreasing in the evolution in inverse time. An example is the Smale – Williams attractor, which arises in the state space of a system if a torus-form region undergoes in one discrete time step a two-fold longitudinal stretching, transverse compression and folding in a double loop located inside the initial torus. With each repetition of the transformation, the number of curls doubles and in the limit tends to infinity, resulting in a so-called solenoid with a characteristic Cantor-like transverse structure. An obvious generalization is construction, where at one step the folded loop has a different number of turns – three or more. Chaotic nature of the dynamics is determined by the fact that the transformation of the angular coordinate in this setup corresponds to an expanding circle map, or the Bernoulli map, of the form $\theta_{n+1} = M\theta_n \pmod{2\pi}$, where $M \geq 2$.

Uniformly hyperbolic attractors are characterized by roughness, or structural stability, by virtue of which the generated chaos retains its features under small variations of the system parameters; obviously, this property is desirable and preferable from the point of view of any plausible application of chaos [6]. A disappointment was that as years passed, it became clear that examples of chaotic systems of different nature, which were considered, do not fit into the narrow frame of the basic hyperbolic theory. In this situation, the hyperbolic dynamics began to be considered only as a refined abstract image of chaos rather than something relating directly to real systems. The deficit of physical examples was overcome in part only very recently [7,8], as instead of searching for "ready-to-use" objects with hyperbolic chaos in nature and technology, we turned to a purposeful design of such systems, applying tools of physics and theory of oscillations, as an alternative to the mathematical exercises based on topological, geometric, and algebraic constructions.

Undoubtedly, from the point of view of clarity, among possible examples of hyperbolic chaos we should outline systems of mechanical nature as they are easily perceived and interpreted in a frame of our everyday experience [9]. In this article, we propose to consider a mechanical system based on two Froude pendulums placed on a common shaft rotating at a constant angular velocity been alternately braked by periodic application of frictional forces. As

we shall show, with proper specification of the system parameters, the Smale-Williams solenoid occurs as an attractor of the Poincaré stroboscopic map. Apparently, this system can be implemented in experiment.

In Section 1 we recall a model of the Froude pendulum, emphasizing the parameter dependence of the frequency of self-oscillations, which is essential for further considerations. In Section 2 we turn to constructing a system based on two pendulums, which can manifest a hyperbolic chaotic attractor. Equations of the mathematical model are formulated, and the operating principle of the system that determines presence of the Smale-Williams attractor in the map describing the state transformation is explained. Section 3 presents numerical results of simulating dynamics of the system; particularly, waveforms of oscillations and portraits of attractors are presented and discussed in various dynamical regimes, analysis of Lyapunov exponents is carried out, and diagrams illustrating transformation of the oscillation phases at successive stages of activity of the pendulums are depicted. We also present results of verification of the hyperbolicity of the attractor at appropriate selection of the system parameters by analyzing angles of intersection of stable and unstable invariant subspaces, confirming the absence of tangencies of these subspaces.

1. Froude pendulum

The Froude pendulum (Fig. 1a) is a good old example of mechanical self-oscillations [10-14]. Consider a weight of mass m on a rod of length l of negligible mass. The rod is attached to a sleeve placed on a shaft rotating at a constant angular velocity Ω . The equation of motion has the form

$$ml^2\ddot{x} + \alpha\dot{x} + mgl \sin x = M(\Omega - \dot{x}). \quad (1)$$

Here x is an angle of the pendulum displacement from the vertical, α is a coefficient of viscous friction with the surrounding medium, l is the distance from the rotation axis to the center of mass, g is the gravity constant, $M(\Omega - \dot{x})$ is moment of the dry friction force between the shaft and the sleeve depending on the value of the relative angular velocity. The form of the dependence is assumed to look like shown in the figure in the separate panel being represented by a curve with decrease having an inflection point.

As is often assumed in construction of the mathematical model, we suppose that the angular velocity of rotation of the shaft Ω is chosen corresponding to the inflection point, and write the expansion of the function in a Taylor series near this point:

$$M(\Omega - \dot{x}) \approx M(\Omega) - M'(\Omega)\dot{x} - \frac{1}{6}M'''(\Omega)\dot{x}^3 = M_0 + A\dot{x} - B\dot{x}^3. \quad (2)$$

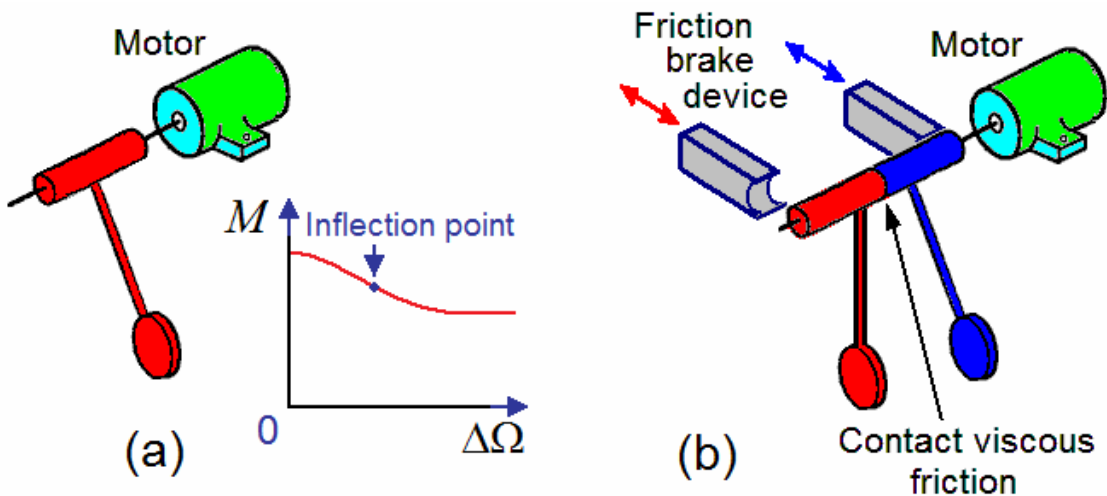


Figure 1: Classic Froude pendulum (a) and system of two such pendulums equipped with a mechanism of alternating braking (b)

Then the equation takes the form

$$\ddot{x} - \frac{A-\alpha}{ml^2} \dot{x} + \frac{B}{ml^2} \dot{x}^3 + \frac{g}{l} \sin x = \frac{M_0}{ml^2}. \quad (3)$$

When introducing the dimensionless quantities

$$t' = \omega_0 t = t \sqrt{\frac{g}{l}}, \quad d = \frac{\alpha}{ml^2 \omega_0}, \quad a = \frac{A}{ml^2 \omega_0}, \quad b = \frac{B \omega_0}{ml^2}, \quad \mu = \frac{M_0}{ml^2 \omega_0^2} \quad (4)$$

we obtain

$$\ddot{x} - (a - d - b\dot{x}^2)\dot{x} + \sin x = \mu. \quad (5)$$

Now the dot denotes differentiation with respect to the dimensionless time t' , and the prime will always be omitted in further notations.

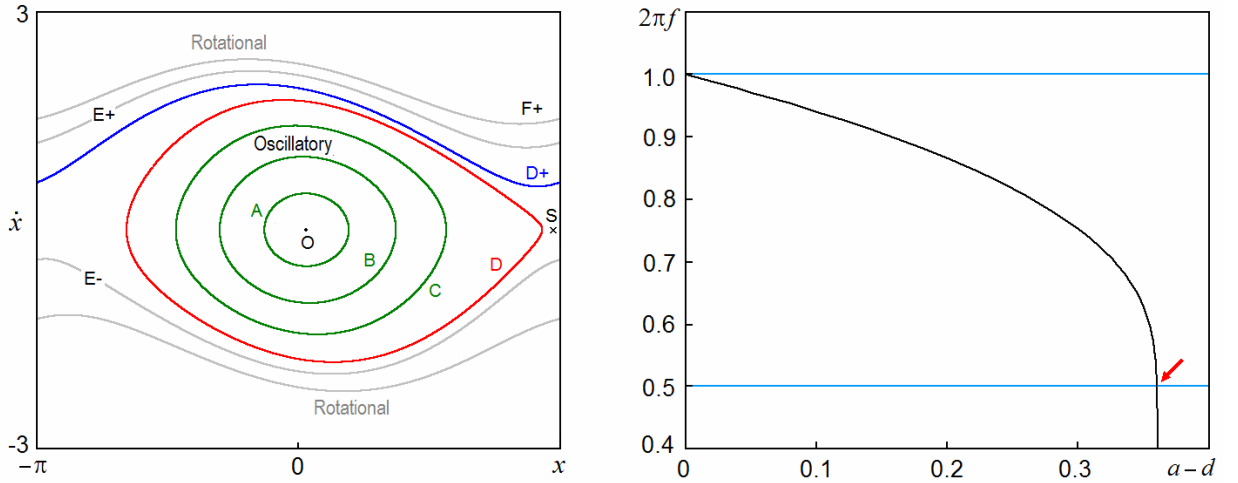


Figure 2: (a) Attracting limit cycles for various parameters corresponding to sustained periodic motions a single Froude pendulum: oscillatory A, B, C, D, respectively, at $a-d = 0.03, 0.12, 0.24, 0.36$, with frequencies $2\pi f = 0.982, 0.926, 0.827, 0.50$, and rotational D+, E±, F±, at $a-d = 0.36, 0.48, 0.60$, with frequencies $1.201(D+), 1.622(E+), 1.044(E-), 1.88(F+), 1.66(F-)$. (b) The dependence of the frequency of the oscillator regimes on the value of $a-d$. Other parameters are $b = 0.16, \mu = 0.087$. On the panel (a) points are marked that are equilibrium states: unstable focus O and saddle S. On the panel (b) the arrow indicates the situation where the frequency of self-oscillations is half the frequency of small oscillations of the pendulum.

If $a-d > 0$, then self-oscillations arise in the system. On the phase plane (Fig. 2a) at each particular parameter value the self-oscillatory mode is represented by an attractive closed trajectory (limit cycle) around the equilibrium state O at $(x, \dot{x}) = (\arcsin \mu, 0)$. For small amplitude, a frequency of the self-oscillations is close to the natural frequency of the oscillator $f = (2\pi)^{-1}$. With growth of $a-d$, the limit cycle increases in size, and the frequency f decreases. This is due to the fact that at the maximum angle the pendulum approaches ever closer and closer to the unstable state corresponding to the position pointing upwards, the saddle point S, $(x, \dot{x}) = (\pi - \arcsin \mu, 0)$, where the motion along the phase trajectory slows down. Further growth of the parameter leads to a change of the oscillatory movements of the pendulum to periodic rotational motions, which correspond to the limit cycles closing as they go around the phase cylinder, and their frequencies are much higher.

For our further consideration, it is essential to select parameters in such a way that the frequency of self-oscillations is exactly half the frequency of small oscillations. At $\mu = 0.087$ and $b = 0.16$ this is the case if we set $a-d = 0.360$. The oscillatory process that arises here contains an essential second harmonic of the fundamental frequency (this is due to the lack of symmetry

of the equation with respect to the substitution $x \rightarrow -x$). If the generated signal acts a linear oscillator of natural frequency $\omega_0 = 1$, one can observe its resonant buildup under the effect of the second harmonic of the self-oscillating system. This is illustrated by Fig. 3, which is plotted basing on the results of numerical integration of the equations

$$\ddot{x} - (a - bx^2)\dot{x} + \sin x = \mu, \quad \ddot{y} + y = \varepsilon\dot{x}. \quad (6)$$

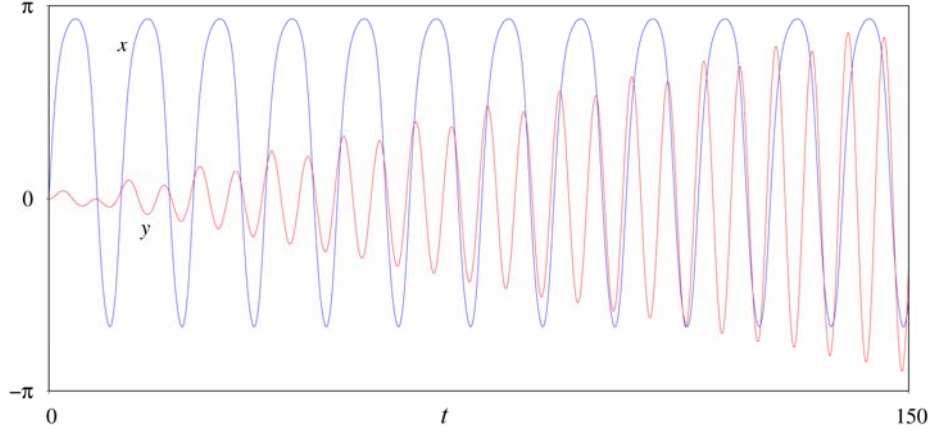


Figure 3: Resonant buildup of a linear oscillator under the action of the second harmonic of the self-oscillatory model of Froude pendulum as obtained from numerical integration of (6) with parameters $a=0.36, b=0.16, \mu=0.087, \varepsilon=0.06$.

2. System based on two coupled pendulums with alternating braking

Let us consider two identical Froude pendulums placed on a common shaft and weakly connected with each other by viscous friction, so that the torque of the frictional force is proportional to the relative angular velocity. Let the motion of one and the other pendulum is decelerated alternately by attaching a brake shoe providing suppression of the self-oscillations due to the incorporated sufficiently strong viscous friction. Denoting the angular coordinate of the first and the second pendulum as x and y , and the angular velocities as u and v , we write down the equations

$$\begin{aligned} \dot{x} &= u, & \dot{u} &= [a - d(t) - bu^2]u - \sin x + \mu + \varepsilon(v - u), \\ \dot{y} &= v, & \dot{v} &= [a - d(t + T/2) - bv^2]v - \sin y + \mu + \varepsilon(u - v), \end{aligned} \quad (7)$$

$$d(t) = \begin{cases} 0, & t < T_0, \\ D, & T_0 < t < T/2, \\ 0, & T/2 < t < T. \end{cases} \quad d(t+T) = d(t).$$

Parameters are assigned as follows:

$$a = 0.36, b = 0.16, \mu = 0.087, \varepsilon = 0.0003, D = 0.8, T = 250, T_0 = T/4. \quad (8)$$

To explain the functioning of the system, let's start with the situation when one pendulum exhibits self-oscillation, and the second is braked. Due to the fact that the parameters are chosen in accordance with the reasoning at the end of the previous section, the basic frequency of the self-oscillatory mode is half of that of the second oscillator. Therefore, when the brake of the second pendulum is switched off, it will begin to swing in a resonant manner due to the action of the second harmonic from the first pendulum, and the phase of the oscillations that arise will correspond to the doubled phase of the oscillations of the first pendulum. As a result, when the second pendulum approaches the sustained self-oscillatory state, its phase appears to be doubled in comparison with the initial phase of the first pendulum. Further, the first pendulum undergoes braking, and at the end of this stage, its oscillations will be stimulated in turn by the action of the second harmonic from the second pendulum, and so on.

Since the system under consideration is non-autonomous, with periodic coefficients, one can go on to description of the dynamics in discrete time using the Poincaré stroboscopic map. In our case, taking into account a symmetry of the system in respect to substitution $x \leftrightarrow y, u \leftrightarrow v, t \leftrightarrow t + T/2$, it is appropriate to use the mapping in half a period of modulation, determining the state vector at the instants of time as

$$\mathbf{X}_n = (x_1, x_2, x_3, x_4)_n = \begin{cases} (x(t_n), u(t_n), y(t_n), v(t_n)), & \text{if } n \text{ is odd,} \\ (y(t_n), v(t_n), x(t_n), u(t_n)), & \text{if } n \text{ is even.} \end{cases} \quad (9)$$

The Poincaré map

$$\mathbf{X}_{n+1} = \mathbf{F}_{T/2}(\mathbf{X}_n) \quad (10)$$

may be easily implemented as a computer program that integrates equations (2) on a half-period of modulation.

Since in the process of the system functioning each new stage of the excitation transfer to one or another pendulum is accompanied by a doubling of the phase of oscillations, this corresponds to the expanding circle map (Bernoulli map) for the phase. If a volume contraction takes place along the remaining directions in the state space of the system, this will correspond to occurrence of the Smale-Williams solenoid as attractor of the Poincaré map (10).

3. Numerical results

Fig. 4 shows waveforms for the angular coordinates of the first and second pendulums on time, which are obtained by numerical integration of equations (7) and illustrate the functioning of the system in accordance with the mechanism described in the previous section.

The observed sustained motion of the system is in fact chaotic, since the oscillation phases in the successive stages of activity vary, obeying the expanding circle map. We are going to illustrate it now, but it should be noted first that in the region of the high-amplitude oscillations their shape differs significantly from the sinusoidal. In this case, evaluation of the phase through the ratio of the variable and its derivative as arctangent is not so satisfactory, and an alternative method of the phase determination is needed. It is appropriate to define the phase using a value of the time shift of the waveform with respect to a given reference point, normalized to the characteristic period of the self-oscillatory mode. Let t be a time instant fixed relative to the modulation profile in the activity region of one of the pendulums, and t_1, t_2 are the preceding moments of the sign change of the angular velocity from plus to minus, and $t_2 > t_1$. Then we can define the phase as a variable belonging to the interval $[0, 1]$ by the relation $\varphi = (t - t_2)(t_2 - t_1)^{-1}$.

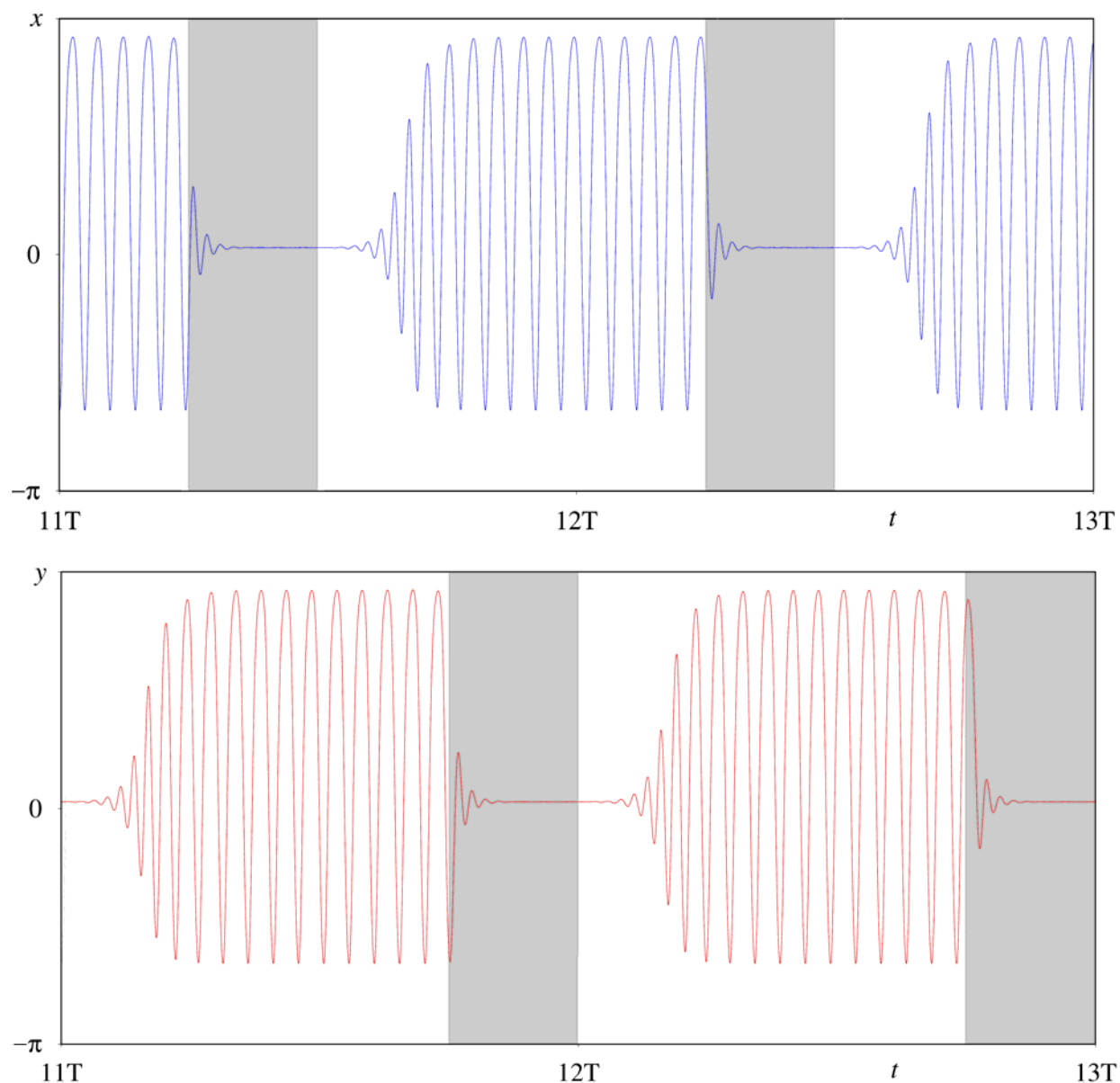


Figure 4: Waveforms of the angular coordinates of the first and second pendulums obtained by numerical integration of equations (7) with parameters (8). The gray bars correspond to the time intervals where the pendulums are subjected to braking

Fig. 5 shows a diagram for the phases determined at the end parts of successive stages of excitation of the first and second pendulums, obtained in numerical calculations for a sufficiently large number of the modulation periods. As can be seen, the mapping for the phase in the topological sense looks equivalent to the Bernoulli map $\varphi_{n+1} = 2\varphi_n + \text{const} \pmod{1}$. Indeed, one complete round for the pre-image φ_n (i.e., a unit shift) corresponds to a double round for the image φ_{n+1} .

Some distortion of the resulting function are related to details of the dynamics, which were not captured within the framework of the given above qualitative description, and they do not play a significant role due to the inherent structural stability of the dynamics under study.

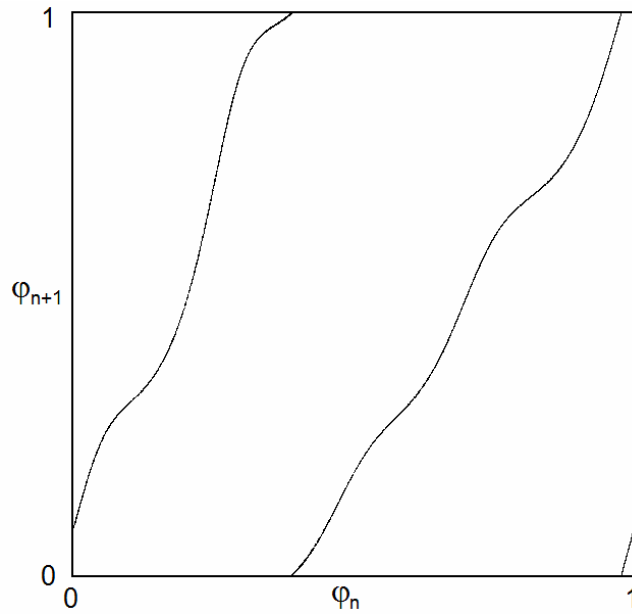


Figure 5: A diagram illustrating transformation of the phases of pendulums in successive stages of activity every half a period of modulation

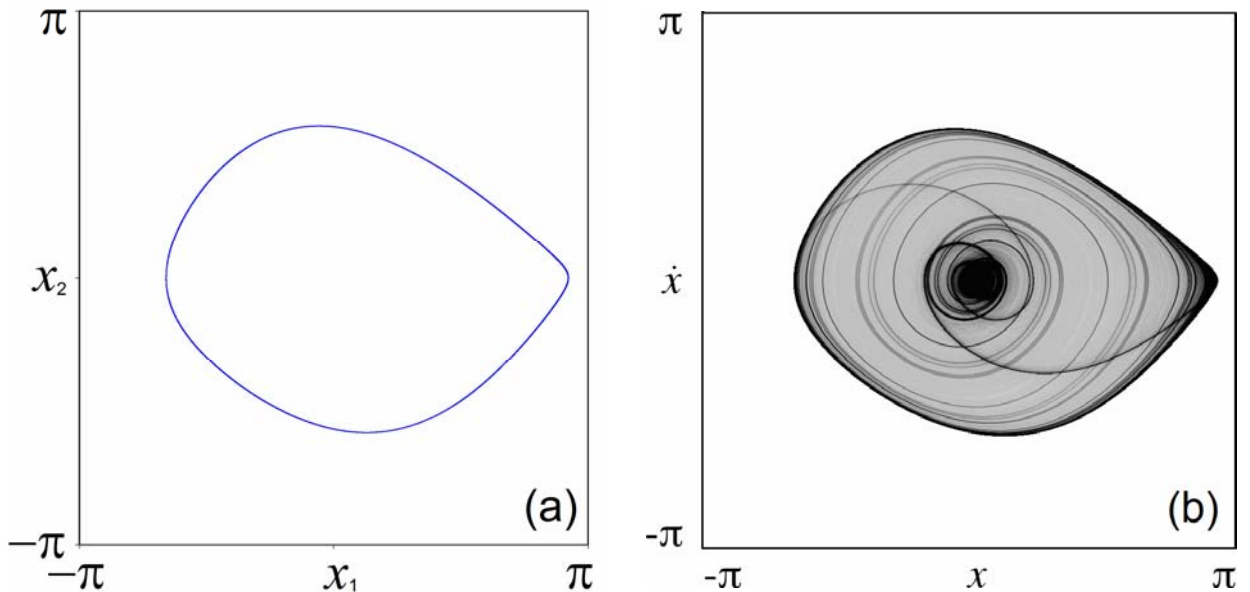


Figure 6: Attractor of the Poincaré stroboscopic map, which is a Smale-Williams solenoid in projection onto the plane of two of variables defined by (9) (a), and attractor of the system with continuous time (7) in the projection from the extended phase space onto the phase plane of the first pendulum (b)

Figure 6a shows attractor of the Poincaré stroboscopic map. Although visually the object looks like a closed curve, in fact it has a fine transverse structure, visualization of which requires accurate high-accuracy calculations, and evolution in discrete time corresponds to jumps of the representing point around the loop accordingly to iterations of the Bernoulli map. Figure 6b shows attractor of the system with continuous time in projection from the extended phase space to the phase plane of the first oscillator. The portrait is represented in the technique of the gray color imaging. At each step of integrating the equations, at corresponding coordinates the gray tone is assigned determined in such way that the number encoding this tone increases every time by one as the point hits the respective pixel.

To obtain spectrum of Lyapunov exponents, we use the traditional algorithm [15-17] and perform numerical integration of equations (7) by a finite-difference method together with a collection of four sets of variation equations

$$\begin{aligned}\dot{\tilde{x}} &= \tilde{u}, & \dot{\tilde{u}} &= [a - d(t) - 3bu^2]\tilde{u} - \tilde{x} \cos x + \varepsilon(\tilde{v} - \tilde{u}), \\ \dot{\tilde{y}} &= \tilde{v}, & \dot{\tilde{v}} &= [a - d(t + T/2) - 3bv^2]\tilde{v} - \tilde{y} \cos y + \varepsilon(\tilde{u} - \tilde{v}),\end{aligned}\quad (11)$$

and the procedure is complemented by the normalization and Gram – Schmidt orthogonalization of the four perturbation vectors $\tilde{\mathbf{x}}^{(i)} = (\tilde{x}_1, \tilde{x}_2, \tilde{x}_3, \tilde{x}_4)_n^{(i)}$, $i=1,2,3,4$ obtained at each half-period $T/2$ using the definition (9). The Lyapunov exponents are evaluated as the average rates of growth or decrease of the accumulating sums of logarithms of the norms for the perturbation vectors before the normalizations. According to the results of the calculations, the parameters specifying according to (8) the Lyapunov exponents for the Poincaré map attractor are the following¹

$$\Lambda_1 = 0.650 \pm 0.007, \quad \Lambda_2 = -5.89 \pm 0.02, \quad \Lambda_3 = -9.46 \pm 0.02, \quad \Lambda_4 = -20.73 \pm 0.02.$$

The presence of a positive exponent Λ_1 indicates chaotic nature of the dynamics. Its value is close to a constant equal to $\ln 2 = 0.693\dots$, which agrees with the approximate description of the evolution of the phase variable φ by the Bernoulli map. The action of the Poincaré map \mathbf{F} in four-dimensional space is accompanied by stretching in the direction corresponding to the dynamical variable associated with the phase φ and contracting along the remaining three directions. This just corresponds to the Smale-Williams construction, namely, in the four-dimensional space. Because of large absolute values of the negative Lyapunov exponents, the transverse structure of fibers of the attractor is indistinguishable in Fig. 6a. An estimate of the Kaplan – Yorke dimension [18] from the spectrum of Lyapunov exponents for this attractor gives $D = 1 + \Lambda_1 / |\Lambda_2| \approx 1.11$.

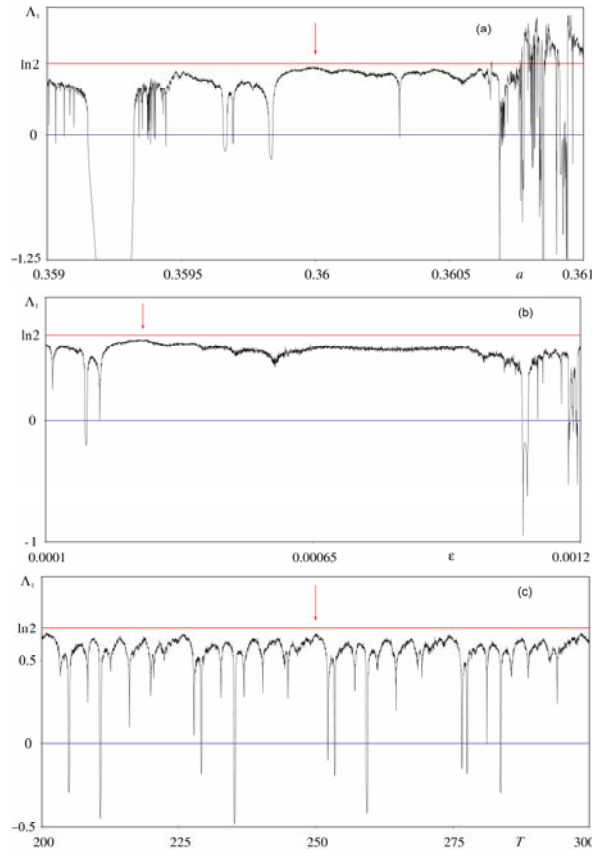


Figure 7: Graphs for the largest Lyapunov exponent of the Poincaré map versus the parameters a (a), ε (b) and T (c). An arrow indicates situation corresponding to the Smale-Williams attractor discussed in the previous section, with parameters assigned according to (8).

¹ The exponents were obtained by averaging over 10^3 samples, each of which corresponded to evaluation of the Lyapunov exponents over $25 \cdot 10^3$ iterations of the Poincaré map. As error bars, the root-mean-square deviations are indicated found by processing the data for this sample space.

In accordance with the expected structural stability, the same type of chaotic attractor should persist under variation of system parameters in some region, and this is indeed the case. Fig. 7 shows graphs of Lyapunov exponents versus parameters a , ε , T . As can be seen, in a neighborhood of the point corresponding to the parameter set (8) there is a region where the positive Lyapunov exponent Λ_1 of the Poincaré map remains close to $\ln 2$. In the same region, as can be verified, correspondence in the topological sense with the Bernoulli map persists for the iteration diagrams for the phases (like in Fig. 5). Appearance of significant deviations of Λ_1 from $\ln 2$, including drops to negative values ("windows of regularity") indicates violation of the hyperbolicity. Note that the width of the hyperbolicity region with respect to the parameter a is rather small because of the strong dependence of the frequency of self-oscillations on this parameter nearby the operating point while the mechanism of the system functioning with resonant energy transfer between the alternately excited oscillators is critical to the ratio of the frequencies for small and large amplitudes 2:1.

Fig. 8 shows other species of attractors occurring in our system of alternately excited Froude pendulums outside the parameter region of the hyperbolic chaos. In the figure caption, the Lyapunov exponents are listed, which make it possible to identify the types of the attractors. Fig. 8a corresponds to a periodic mode associated with attracting limit cycle in the phase space of the system, and in the Poincaré map the attractor consists of three points visited in turn. All the Lyapunov exponents are negative. Fig. 8b corresponds to a quasi-periodic motion, which in the Poincaré section is represented by a smooth closed invariant curve. The largest Lyapunov exponent is zero (up to an error of the computations), and the remaining exponents are negative. Fig. 8c depicts a nonhyperbolic chaotic attractor, in which one Lyapunov exponent is positive (significantly different from $\ln 2$), and the remaining ones are negative. This attractor corresponds to a chaotic regime of motion of the Froude pendulums accompanied by rotations. Fig. 8d also represents a chaotic mode, in which the movements of the pendulums are of rotational nature, but in this case the attractor has two positive Lyapunov exponents; according to commonly accepted terminology, this is hyperchaos.

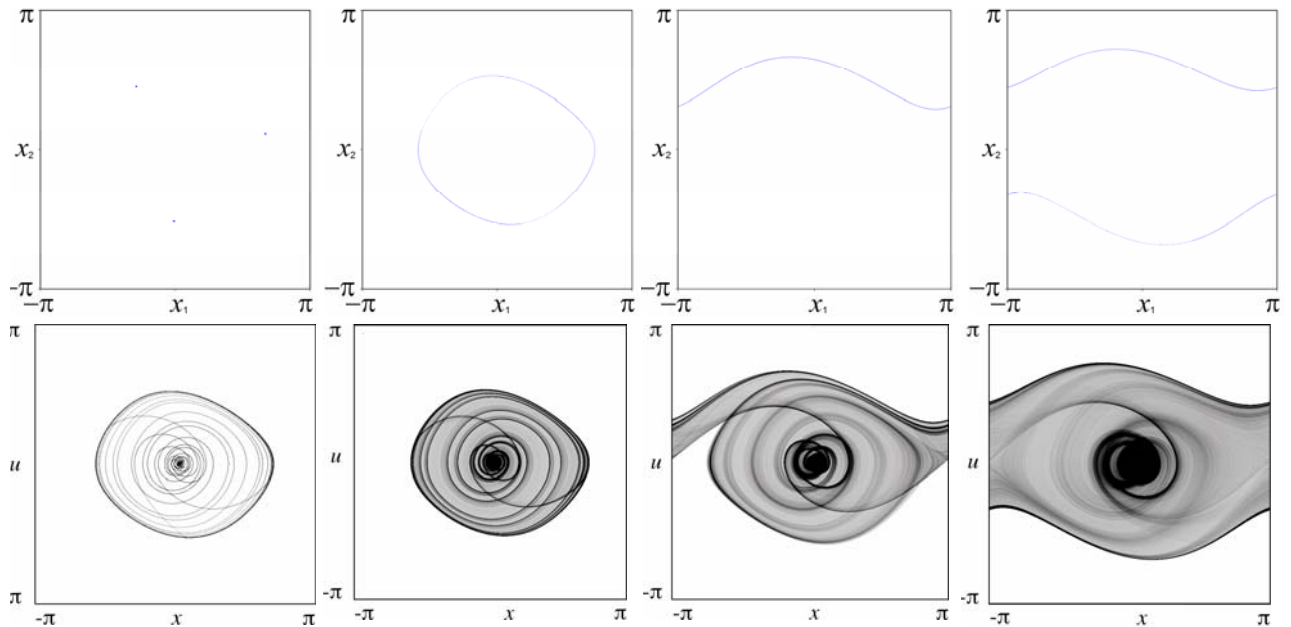


Figure 8: Attractors of the Poincaré stroboscopic map (upper row) and attractors of the continuous time system in projection from the extended phase space onto the phase plane of the first pendulum.

- (a) Periodic mode, $a = 0.31$, $\Lambda = (-0.23, -6.79, -18.05, -24.38)$;
- (b) Quasiperiodic mode, $a = 0.32$, $\Lambda = (0.000, -7.03, -17.34, -24.38)$;
- (c) Chaotic mode, $a = 0.42$, $\Lambda = (1.00, -1.78, -18.62, -32.28)$;
- (d) Hyperchaos, $a = 0.55$, $\Lambda = (0.95, 0.34, -30.09, -31.27)$.

4. Hyperbolicity test

A method for verifying the hyperbolicity proposed in [19, 20] is that for a typical trajectory on an attractor, the linearized variation equations for the perturbation vectors are solved first in direct time to determine the unstable subspace, and then a set of the variation equations is integrated in the inverse time along the same reference trajectory to determine the stable subspace. Further, for a set of points of the trajectory, the angles between these subspaces are evaluated, and their distribution is analyzed. If it is separated from the region of zero angles, it indicates hyperbolic nature of the attractor, whereas the appearance of the angles close to zero indicates that there is no hyperbolicity. This method was applied to a number of specific model systems and allowed confirming the hyperbolic nature of attractors [7-9, 21-24].

In the modified version of the method [25,26,27], which is especially convenient for multidimensional systems, to identify the contracting subspace one deals not with vectors belonging to it, but with vectors defining its orthogonal complement, determined by the conjugate linearized equations.

In our case, the conjugate equations have the form

$$\begin{aligned}\dot{\xi} &= \eta \cos x, \quad \dot{\eta} = [a - d(t) - 3bu^2]\eta + \xi + \varepsilon(\eta - \upsilon), \\ \dot{\zeta} &= \upsilon \cos y, \quad \dot{\upsilon} = [a - d(t + T/2) - 3bv^2]\upsilon + \eta + \varepsilon(\upsilon - \eta).\end{aligned}\quad (12)$$

They are constructed in such way that for the vectors given by the equations (11) and (12), the scalar product defined by the relation

$$\tilde{\mathbf{x}} \cdot \boldsymbol{\xi} = \tilde{x}(t)\xi(t) + \tilde{u}(t)\eta(t) + \tilde{y}(t)\zeta(t) + \tilde{v}(t)\upsilon(t) \quad (13)$$

should be constant in time.

In our case, in the parameter region where the Smale-Williams attractor occurs, the unstable subspace for a trajectory belonging to the attractor is one-dimensional, as well as the orthogonal complement to the stable subspace. First, we perform computations to get a long segment of the reference trajectory of system (7) $x(t)$, $u(t)$, $y(t)$, $v(t)$. Then, along this trajectory, the equations in variations (11) are numerically integrated that gives a vector $\tilde{\mathbf{x}}(t) = (\tilde{x}, \tilde{u}, \tilde{y}, \tilde{v})$ associated with a positive Lyapunov exponent. Further, along the same trajectory in the inverse time, the conjugate equations are integrated that gives the vector $\boldsymbol{\xi}(t) = (\xi, \eta, \zeta, \upsilon)$. At the end of the procedure, the angles are calculated through the scalar product of pairs of vectors related to identical points of the reference trajectory, namely, at time instants corresponding to the Poincaré section, $\beta_n = \arccos \frac{\tilde{\mathbf{x}}_n \cdot \boldsymbol{\xi}_n}{|\tilde{\mathbf{x}}_n| |\boldsymbol{\xi}_n|}$, $\alpha_n = \pi/2 - \beta_n$, and a histogram of their distribution is plotted.

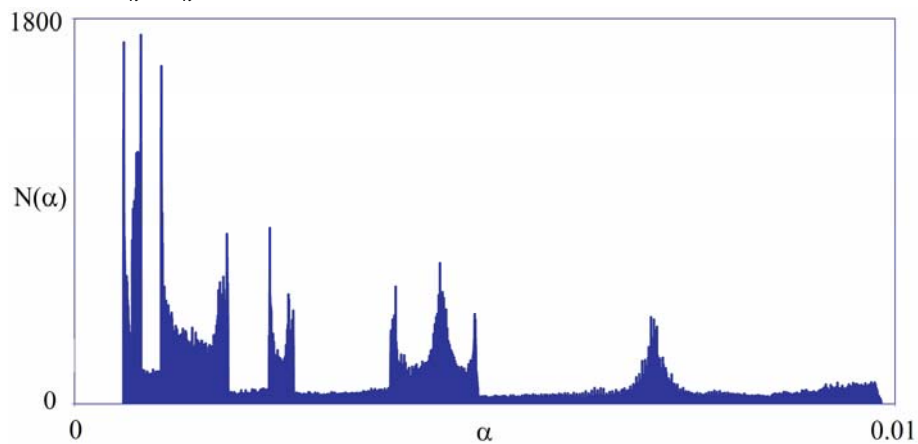


Fig. 9. Histograms of the angles of intersection of stable and unstable subspaces for the hyperbolic attractor of Poincaré map of the system (7)

Fig. 9 shows the histogram of the angles of intersection of stable and unstable subspaces for a trajectory on the attractor of the Poincaré map of the system with parameters assigned

according to (8). The fact that the distribution is separated from zero, confirms the hyperbolic nature of the attractor. Similar results are obtained for parameters of the system in a certain range, which corresponds to the inherent roughness (structural stability) inherent to the hyperbolic attractor.

Conclusion

We have proposed a new example of a mechanical oscillator with hyperbolic chaotic attractor. The system is constructed on the basis of two connected Froude pendulums on a common shaft rotating at constant angular velocity, and they are alternately damped by periodic application of the additional friction. A mathematical model is formulated and its numerical study is carried out. It is shown that, with appropriate specification of the parameters, attractor of the Poincaré stroboscopic map is a Smale-Williams solenoid. The hyperbolicity of the chaotic attractor is confirmed with the help of a criterion based on analysis of angles of intersection of stable and unstable invariant subspaces of small perturbation vectors with verification of the absence of tangencies between these subspaces.

The material presented is interesting, first, in a sense of filling the hyperbolic theory, a deeply developed and advanced section of the modern theory of dynamical systems, which gives a rigorous justification for the presence of structurally stable chaos, with the physical content.

The proposed system, apparently, allows implementation as a simple mechanical device, which would allow an experimental study of hyperbolic chaos. Due to visibility of the dynamics of the system, which is a mechanical object, this kind of experiment could be useful, particularly, in practical laboratory studies for graduate and post-graduate students specializing in the field of nonlinear dynamics.

The approach considered here can serve as example for constructing a wide class of objects of various nature that demonstrate hyperbolic attractors on the basis of subsystems, the transfer of oscillatory excitation between which take place in resonance due to special selection of the integer ratio of frequencies of small and large oscillations. For example, it can be done for a system of two Bonhoeffer-van der Pol electronic oscillators with external control so that they alternately undergo damping or excitation of relaxation oscillations whose frequency is twice or three times smaller than the frequency of small oscillations [28].

The work was supported by the grant of Russian Science Foundation No. 15-12-20035.

References

- [1] Smale S. Differentiable dynamical systems // Bull. Amer. Math. Soc. (NS). 1967. V. 73. P. 747-817.
- [2] Anosov D.V., Gould G.G., Aranson S.K., Grines V.Z., Plykin R.V., Safonov A.V., Sataev E.A., Shlyachkov S.V., Solodov V.V., Starkov A.N., Stepin A.M.. Dynamical Systems IX: Dynamical Systems with Hyperbolic Behaviour (Encyclopaedia of Mathematical Sciences) (v. 9). Springer, 1995.
- [3] Katok A. and Hasselblatt B. Introduction to the Modern Theory of Dynamical Systems. Cambridge: Cambridge University Press, 1995.
- [4] Shilnikov L. Mathematical problems of nonlinear dynamics: a tutorial International Journal of Bifurcation and Chaos. 1997. V. 7. No 9. P. 1953-2001
- [5] Anosov D.V. Dynamical Systems in the 1960s: The Hyperbolic Revolution // Mathematical Events of the Twentieth Century, Berlin Heidelberg: Springer-Verlag and Moscow: PHASIS, 2006. P. 1-18.
- [6] Elhadj Z., Sprott J. C. Robust Chaos and Its Applications. Singapore: World Scientific, 2011. 472p.
- [7] Kuznetsov S.P. Dynamical chaos and uniformly hyperbolic attractors: from mathematics to physics //Physics-Uspekhi. 2011. V. 54. No 2. P. 119-144.
- [8] Kuznetsov S.P. Hyperbolic Chaos: A Physicist's View. Higher Education Press: Beijing and Springer-Verlag: Berlin, Heidelberg, 2012, 336p.
- [9] Kuznetsov S.P., Kruglov V.P. On Some Simple Examples of Mechanical Systems with Hyperbolic Chaos. Proceedings of the Steklov Institute of Mathematics, **297**, 2017, 208–234.
- [10] John William Strutt Baron Rayleigh, Robert Bruce Lindsay. The Theory of Sound, Tom 1. Courier Corporation, 1945. 520p.

- [11] Strelkov S.P. The Froude pendulum //Zh. Tekh. Fiz. – 1933. – T. 3. – №. 4. – C. 563-573.
- [12] Landa P.S. Nonlinear oscillations and waves in dynamical systems. – Springer Science & Business Media, 2013.
- [13] Anishchenko V.S., Vadivasova T., Strelkova G. Deterministic Nonlinear Systems. – Springer International Publishing Switzerland, 2014.
- [14] Dai L., Singh M.C. Periodic, quasiperiodic and chaotic behavior of a driven Froude pendulum //International journal of non-linear mechanics. – 1998. – T. 33. – №. 6. – C. 947-965.
- [15] Benettin G., Galgani L., Giorgilli A., & Strelcyn J. M. (1980). Lyapunov characteristic exponents for smooth dynamical systems and for Hamiltonian systems; a method for computing all of them. Part 1: Theory. *Meccanica*, 15(1), 9-20.
- [16] Shimada I., Nagashima T. A numerical approach to ergodic problem of dissipative dynamical systems //Progress of theoretical physics. – 1979. – T. 61. – №. 6. – C. 1605-1616.
- [17] Pikovsky A., Politi A. Lyapunov exponents: a tool to explore complex dynamics. – Cambridge University Press, 2016.
- [18] Kaplan J.L. and Yorke J.A. A chaotic behavior of multi-dimensional differential equations //Peitgen H.-O. and Walther H.-O. (eds.) *Functional Differential Equations and Approximations of Fixed Points*. Lecture Notes in Mathematics. V. **730**. Berlin, N.Y.: Springer, 1979. P. 204–227.
- [19] Lai Y.C., Grebogi C., Yorke J.A., Kan I. How often are chaotic saddles nonhyperbolic? *Nonlinearity*, 6, 1993, No 5, 779-797.
- [20] Anishchenko V.S., Kopeikin A.S., Kurths J., Vadivasova T.E., Strelkova G.I. Studying hyperbolicity in chaotic systems. *Physics Letters A*, 270, 2000, 301-307.
- [21] Kuznetsov S.P. Example of a Physical System with a Hyperbolic Attractor of the Smale-Williams Type. *Phys. Rev. Lett.*, **95**, 2005, 144101.
- [22] Kuznetsov S.P., Seleznev E.P. A strange attractor of the Smale–Williams type in the chaotic dynamics of a physical system. *JETP* **102**, 2006, No. 2, 355-364.
- [23] Kuznetsov S.P. Hyperbolic Chaos in Self-oscillating Systems Based on Mechanical Triple Linkage: Testing Absence of Tangencies of Stable and Unstable Manifolds for Phase Trajectories. *Regular and Chaotic Dynamics*, **20**, 2015, No 6, 649–666.
- [24] Kuznetsov S.P. and Kruglov V.P. Verification of hyperbolicity for attractors of some mechanical systems with chaotic dynamics // *Regular and Chaotic Dynamics*, 2016, Vol. 21, No. 2, 160–174.
- [25] Kuptsov P.V. Fast numerical test of hyperbolic chaos. *Phys. Rev. E*, 85, 2012, No 1, 015203.
- [26] Kuptsov P.V. and Kuznetsov S.P. Numerical test for hyperbolicity of chaotic dynamics in time-delay systems. *Phys. Rev. E*, **94**, 2016, No 1, 010201.
- [27] Kuptsov P.V., Kuznetsov S.P. Numerical test for hyperbolicity in chaotic systems with multiple time delays. *Communications in Nonlinear Science and Numerical Simulation*, **56**, 2018, 227-239.
- [28] Kruglov V.P., Doroshenko V.M., Kuznetsov S.P. Hyperbolic chaos in the coupled Bonhoeffer -van der Pol oscillators operating with excitation of relaxation self-oscillations. *Nonlinear Waves – 2018. XVIII Scientific School. Abstracts of Reports of Young Scientists*. IAP RAS, Nizhny Novgorod, 2018. Pp. 87-89. http://www.nonlinearwaves.sci-nnov.ru/images/Tezis_NV-2018-n1.pdf. (In Russian.)